

Starbursting Brightest Cluster Galaxy: a *Herschel* view of the massive cluster MACS J1931.8–2634

J. S. Santos^{1*}, I. Balestra², P. Tozzi¹, B. Altieri³, I. Valtchanov³, A. Mercurio⁴, M. Nonino², Heng Yu^{5,6,7}, P. Rosati⁸, C. Grillo⁹, E. Medezinski^{10,11}, A. Biviano²

¹ INAF - Osservatorio Astrofisico di Arcetri, Largo Enrico Fermi 5, 50125 - Firenze, Italy

² INAF - Osservatorio Astronomico di Trieste, Via Tiepolo 11, 34131 - Trieste, Italy

³ European Space Astronomy Centre (ESAC)/ESA, Villanueva de la Cañada, 28691, Madrid, Spain

⁴ INAF - Osservatorio Astronomico di Capodimonte, Salita Moiarriello 16, 80131 - Napoli, Italy

⁵ Department of Astronomy, Beijing Normal University, Beijing, 100875 China

⁶ Dipartimento di Fisica, Università di Torino, Via P. Giuria 1, I-10125 Torino, Italy

⁷ Istituto Nazionale di Fisica Nucleare (INFN), Sezione di Torino, Via P. Giuria 1, 10125 Torino, Italy

⁸ Department of Physics and Earth Science, University of Ferrara, Via Saragat, 1, 44122 Ferrara, Italy

⁹ Dark Cosmology Centre, Niels Bohr Institute, University of Copenhagen, Juliane Maries Vej 30, DK-2100 Copenhagen, Denmark

¹⁰ Center for Astrophysics and Planetary Science, Racah Institute of Physics, The Hebrew University, Jerusalem 91904, Israel

¹¹ Department of Physics and Astronomy, The Johns Hopkins University, 3400 North Charles Street, Baltimore, MD 21218, USA

Accepted Received ...;

ABSTRACT

We investigate the dust-obscured star formation properties of the massive, X-ray selected galaxy cluster MACS J1931.8–2634 at $z=0.352$. Using far-infrared (FIR) imaging in the range 100–500 μm obtained with the *Herschel* telescope, we extract 31 sources (2σ) within $r \sim 1$ Mpc from the brightest cluster galaxy (BCG). Among these sources we identify six cluster members for which we perform an analysis of their spectral energy distributions (SEDs). We measure total infrared luminosity (L_{IR}), star formation rate (SFR) and dust temperature. The BCG, with $L_{\text{IR}}=1.4 \times 10^{12} L_{\odot}$ is an Ultra Luminous Infrared Galaxy and hosts a type II AGN. We decompose its FIR SED into AGN and starburst components and find equal contributions from AGN and starburst. We also recompute the SFR of the BCG finding $\text{SFR}=150 \pm 15 \text{ M}_{\odot} \text{yr}^{-1}$. We search for an isobaric cooling flow in the cool core using *Chandra* X-ray data, and find no evidence for gas colder than 1.8 keV in the inner 30 kpc, for an upper limit to the instantaneous mass-deposition rate of $58 \text{ M}_{\odot} \text{yr}^{-1}$ at 95% c.l. This value is $3 \times$ lower than the SFR in the BCG, suggesting that the on-going SF episode lasts longer than the ICM cooling events.

Key words: galaxies: clusters: individual: MACS J1931.8–2634; galaxies: star formation; infrared: galaxies; X-rays: galaxies: clusters

1 INTRODUCTION

The cores of galaxy clusters are ubiquitously populated by old, passively evolving spheroids, with little evidence for ongoing or recent episodes of star formation (e.g., Dressler 1980; Dressler et al. 1997; Von der Linden et al. 2010; Girardi et al. 2015). This suppression of star formation (SF) is mainly caused by interactions among the densely packed galaxies (e.g., Moore et al. 1996; Gnedin 2003), and to a lesser extent by interactions between the hot, X-ray emitting intracuster medium (ICM) and the galaxies. The brightest cluster galaxy (BCG) that usually sits at the bottom of the

potential well and is coincident with the peak of the cluster X-ray emission, is typically a very massive, bright, early type galaxy, that only rarely is associated with significant star formation activity (e.g., Samuele et al. 2011; Rawle et al. 2012; Fogarty et al. 2015).

Cool core (CC) clusters are systems whose ICM shows a minimum core temperature that is about one third of the global ICM temperature and a low core entropy ($< 30 \text{ keV cm}^2$), that reflects significant radiative cooling taking place in the cluster innermost regions (e.g., Peterson & Fabian 2006; Hudson et al. 2010). Observations have shown that BCGs with ongoing star formation activity are usually hosted by CC clusters (Hoffer et al. 2012). However, there is still a large variance in current results on the fraction

* E-mail: jsantos@arcetri.astro.it

of star forming BCGs and the amount of their star formation rate (SFR). This is partly because different diagnostics are used (e.g., optical emission lines, UV continuum, far-infrared) that may be affected by dust emission and AGN contamination, but also because samples are often not representative. In particular, Samuele et al. (2011) investigated the star formation activity in a sample of 77 BCGs drawn from a flux limited, X-ray selected cluster sample and reported a lack of star formation in that sample, based only on optical emission lines. In contrast, Rawle et al. (2012) detected star formation in 15 out of 68 BCGs using a more robust diagnostic based on the FIR emission. The caveat in this fraction is that the sample of BCGs originate from a mix of cluster samples, mostly selected to include massive and relaxed clusters that are thus biased toward CCs, therefore are more likely associated with star forming BCGs.

It is well known that AGN play a crucial role in the regulation of the star formation in BCGs (e.g., Hlavacek-Larrondo et al. 2013; Russell et al. 2013). Ample evidence for AGN feedback has been collected in the last decade, where radio jets have been shown to inflate bubbles in the ICM and hence offset cooling, nonetheless the link between AGN and star formation is not yet properly established (e.g., McNamara & Nulsen 2007, for a review). The recent study of the Phoenix cluster at $z=0.596$ (McDonald et al. 2012), the strongest CC cluster known to date, showed a BCG with a very high SFR *and* an equally significant AGN activity.

The X-ray selected cluster MACS J1931.8–2634 (MACS1931 hereafter, Ebeling et al. 2001) at $z=0.352$ is part of the CLASH (Cluster Lensing And Supernova survey with Hubble, Postman et al. 2012) sample of 25 massive clusters used to study the distribution of dark matter in clusters. As all of the CLASH clusters, MACS1931 is massive with $M_{200}=9.9\pm0.7\times10^{14} M_{\odot}$ (Merten et al. 2015) with a relaxed X-ray morphology, and harbors a cool core (Ehlert et al. 2011). The cluster is dominated by a very large, luminous central galaxy that, contrary to what is common in most massive clusters, is undergoing a phase of copious star formation. Measured star formation rates range from $80 M_{\odot}\text{yr}^{-1}$ (rest-frame UV imaging, Donahue et al. 2015) to $170 M_{\odot}\text{yr}^{-1}$ (broad band optical imaging, Ehlert et al. 2011). However, these SFRs may be contaminated by AGN activity and underestimated due to dust obscuration.

The work presented in this Letter aims to overcome these two biases. We present the analysis of *Herschel* (Pilbratt et al. 2010) 100–500 μm observations of MACS1931 that cover the peak of the SED of starbursts. The far-infrared (FIR) is the best diagnostic for star formation as it provides a direct measure of the reprocessed UV light from the on-going star formation, allowing us to measure the total FIR luminosity, star formation rates and dust temperatures of the cluster members. We also focus on the BCG and its environment using *Chandra* X-ray data. The work presented here is part of a larger *Herschel* study including all CLASH clusters. The cosmological parameters used throughout the paper are: $H_0=70 h \text{ km/s/Mpc}$, $\Omega_{\Lambda}=0.7$ and $\Omega_{\text{m}}=0.3$.

2 DATA

Although the present work is focused on data from the *Herschel* space telescope, we use ample ancillary data

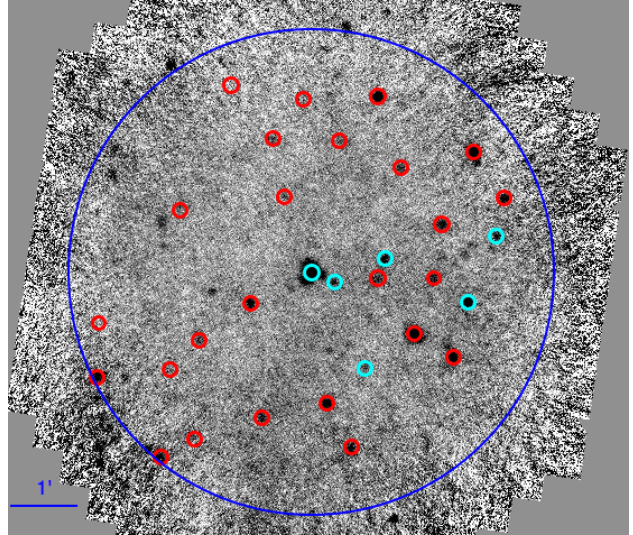


Figure 1. PACS $100\mu\text{m}$ image of the cluster field centered on the BCG. The blue circle with $r \sim 1 \text{ Mpc}$ ($\sim 1/2$ of r_{200}) indicates the region of source extraction. The small ($6''$ radius) circles represent the 31 individual FIR sources in our catalog (cluster members are highlighted in cyan). North is up and East to the left.

both proprietary and archival: mid-infrared data from WISE; X-ray data from *Chandra*; optical data from Subaru (BVR_cI_cz), the *Hubble Space Telescope* (HST), and extensive VLT/VIMOS spectroscopy.

2.1 *Herschel* observations and data reduction

The *Herschel* observations of MACS1931 were carried out in 2011, 2012 and 2013 as Open Time 1 and 2 programmes (PI Egami, obsid = 1342215993, 1342241619, 1342241681, 1342254639) aimed at studying the star formation properties of lensing clusters. The PACS (Poglitsch et al. 2011) observations at 100 and $160\mu\text{m}$ were performed in scan map mode. The maps were produced using Unimap (Piazzo et al. 2015): a Generalized Least Square map-maker, that allows us to reach ultimate sensitivity with no flux loss, and without iterative masking of the sources. The 1σ noise of the maps is 1.6 mJy in the $100 \mu\text{m}$ band and 3.5 mJy in the $160 \mu\text{m}$ image. SPIRE (Griffin et al. 2010) maps with a $\sim 5'$ radius were obtained in small map mode. The SPIRE maps at 250, 350 and $500 \mu\text{m}$ with nominal pixel sizes of $6''$, $10''$ and $14''$, respectively, are dominated by confusion noise with an rms in the center of 6.2, 6.5 and 7.3 mJy .

2.2 Far-infrared sources in MACS1931

Our far-infrared observations of MACS1931 covers a region with $3.6'$ radius centered on the X-ray cluster center, where the sensitivity of the PACS maps is robust (see Fig. 1). This radius corresponds to 1.1 Mpc in physical units which is about $1/2$ of the cluster virial radius measured from lensing ($r_{200}=1.82\pm0.04 \text{ Mpc}$, Merten et al. 2015).

Here we outline our procedure to obtain the catalog of FIR sources in the field of MACS1931. Our catalog is based on blind source detections in the 100 and $160\mu\text{m}$ maps separately, using SExtractor (Bertin & Arnouts 1996). As standard for PACS data, the photometry is made with fixed

Table 1. Properties of the FIR cluster members, with spectroscopic redshift and photometric redshift concordant with the cluster.

ID	RA	DEC	z	r_{proj} kpc	$F_{100\mu m}$ mJy	$F_{160\mu m}$ mJy	LIR $\times 10^{11} L_{\odot}$	SFR $M_{\odot} \text{yr}^{-1}$	T_{dust} K
62	292.905501	-26.5669131	0.3644	923	6.5 ± 1.7	9.6 ± 3.6	0.43 ± 0.04	6.4 ± 0.6	29 ± 5
69 (BCG)	292.956707	-26.5758907	0.352	—	212.5 ± 15.0	231.3 ± 16.5	14 ± 2	210 ± 23	33 ± 2
75*	292.950604	-26.5782649	0.3652	117	3.2 ± 1.6	10.7 ± 3.6	0.47 ± 0.07	7.0 ± 1.5	14 ± 1
89	292.941855	-26.5994976	0.3494	498	4.0 ± 1.6	10.1 ± 3.6	0.34 ± 0.04	5.0 ± 0.5	24 ± 4
68	292.936482	-26.5724383	0.36 ± 0.07	366	8.9 ± 1.7	12.4 ± 3.6	0.54 ± 0.06	8.0 ± 1.0	30 ± 4
80	292.913344	-26.5832069	0.34 ± 0.07	785	21.5 ± 2.2	32.2 ± 4.2	1.3 ± 0.1	19.5 ± 1.7	29 ± 2

* SPIRE fluxes of ID 75 may be contaminated by the BCG that is located at $\sim 20''$ distance.

apertures with radii of $6''$ and $9''$ at $100\mu m$ and $160\mu m$, respectively, corrected with the encircled energy factors given by Balog et al. (2014). This procedure was validated with manual aperture photometry. Given the difficulty to obtain reliable errors with standard source detection algorithms because of the correlated noise present in PACS data, we compute the photometric errors as the 1σ detection limits in each band, in addition to 7% (calibration accuracy of the flux scale) of the source flux. The SPIRE source detection was performed using a simultaneous fit to all sources in the prior list based on the PACS detections. We run the XID method (Roseboom et al. 2012) using the same prior catalog on the three SPIRE bands, using the corresponding SPIRE point response function for each band. If the fitted SPIRE flux density at the position of an input PACS source is below the 3σ sensitivity in each band we assigned the 3σ values as upper limits. These correspond to $3\times$ the confusion noise and are equal to 17.4, 18.9 and 20.4 mJy at 250, 350 and $500\mu m$, respectively.

We obtain 31 detections at $>2\sigma$ in at least one of the PACS bands, within $r=3.6'$ centered on the BCG. To identify the origin of these sources we match the FIR catalog with our spectroscopic and photometric redshift catalogues. The spectroscopic catalog consists of 2800 redshifts obtained with VIMOS (CLASH-VLT Large Programme 186.A-0798, PI Rosati, Rosati et al. 2014), whereas the photo- z catalogues are based on photometry from the HST and Subaru¹. We find that, of the 31 sources in the cluster field, 4 are confirmed members, 2 are candidate members (photo- z) and 18 are interlopers. Since the completeness of our spectroscopic sample of cluster members is close to 90% it is unlikely that the remaining 7 *Herschel* sources are at the cluster redshift.

3 FAR-INFRARED PROPERTIES OF THE CLUSTER GALAXIES

We fit the galaxies FIR SEDs using **LePhare** (Arnouts et al. 1999) with Chary & Elbaz (2001) templates, to measure the galaxy integrated infrared luminosity L_{IR} in the range 8– $1000\mu m$. The star formation rates are derived using the updated scaling relation, $SFR_{IR} = 1.48 \times 10^{-10} L_{IR}/L_{\odot}$, (Kennicutt 2012; Murphy et al. 2011; Hao et al. 2011) that uses a Kroupa initial mass function (Kroupa et al. 2003)². The

SFR of our sample, measured with pure starburst templates, spans the range 5 - $210 M_{\odot} \text{yr}^{-1}$. If we exclude the highest star-forming galaxy - the BCG - we find an average SFR of $9.2 M_{\odot} \text{yr}^{-1}$. The total SFR of the six cluster galaxies amounts to $256 M_{\odot} \text{yr}^{-1}$. This value is in good agreement with the recent result on the SFR of massive clusters using *Herschel* data by Popesso et al. (2015). In the next section we perform a more detailed study of the BCG and refine its SFR measure, after accounting for the impact of the AGN. With the exception of the BCG that is an Ultra Luminous Infrared Galaxy (ULIRG, $\gtrsim 10^{12} L_{\odot}$), the FIR detected cluster galaxies are LIRGs or normal star forming galaxies.

The temperature of the dust, T_{dust} , present in the galaxies is computed with a modified black body model with an emissivity index β fixed to 1.5. Apart from galaxy ID 75, that shows some contamination with the BCG fluxes in the SPIRE bands, we find T_{dust} in the range 24–33 K, which is within the range of dust temperatures for $z \leq 0.3$ LIRGs and ULIRGs (Magdis et al. 2014). The FIR properties of the cluster members are summarized in Table 1.

4 CONNECTION BETWEEN THE BCG, THE AGN AND THE ICM

In this section we analyze in detail the BCG sitting at the core of the cluster. It is uncommon to have a cluster with a massive BCG with a SFR level of $210 M_{\odot} \text{yr}^{-1}$ (Rawle et al. 2012; Hoffer et al. 2012). However, our initial SFR result may be biased by the presence of a strong obscured AGN, which needs to be carefully modeled. We also explore the interconnections between the star formation of the BCG and the mass deposition rate in the cluster core. The UV and optical properties of this galaxy have been studied in Donahue et al. (2015) and Ehlert et al. (2011), that computed the galaxy star formation rate using different diagnostics. We convert their values to the ones obtained with the updated calibration used here, as described in Kennicutt (2012). While Donahue et al. (2015) found a $SFR = 69 M_{\odot} \text{yr}^{-1}$ using UV photometry, Ehlert et al. (2011), in a crude approximation, derived a value twice larger, $146 M_{\odot} \text{yr}^{-1}$, based on optical broad band imaging. These calculations do not account for dust extinction nor for contamination from AGN activity.

4.1 SED decomposition: AGN & star formation

The BCG of MACS1931 hosts an X-ray bright AGN, embedded in the ICM emission, which we model and sub-

¹ CLASH catalogs: <https://archive.stsci.edu/prepds/clash/>

² These SFRs are lower than the ones obtained with the widely used Kennicutt 1998 calibration ($SFR=0.86 \times SFR_{K98}$)

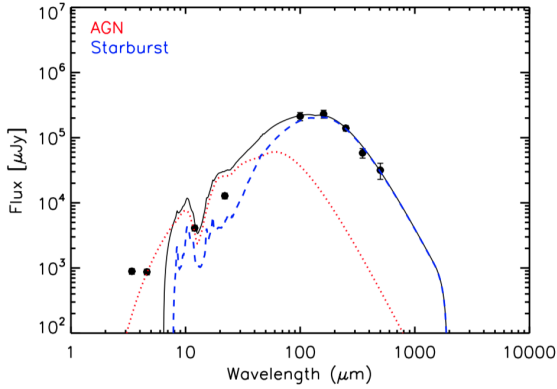


Figure 2. Infrared SED of the BCG. Black points show the observed data from WISE and *Herschel* and the black solid line represents the best-fit SED model. AGN and starburst components from the combined SED are shown in red and blue, respectively.

tract from the AGN signal. We detect about 1030 counts in the 0.5–7 keV band. Our spectral analysis with an intrinsic slope fixed to $\Gamma = 1.8$, provides an intrinsic absorption of $N_H = 1.94^{+0.21}_{-0.19} \times 10^{22} \text{ cm}^{-2}$, which is very close to the canonical value 10^{22} cm^{-2} above which an AGN is classified as absorbed. The unabsorbed rest-frame luminosities are $L_{0.5-2\text{keV}} = 3.6 \times 10^{43} \text{ ergs s}^{-1}$ and $L_{2-10\text{keV}} = 6.9 \times 10^{43} \text{ ergs s}^{-1}$.

We first investigate the contribution of the AGN component to the FIR emission using **DecompIR** (Mullaney et al. 2011), an SED model fitting software that decomposes the FIR SED in AGN and starburst components. In short, the AGN component is an empirical model based on observations of moderate-luminosity local AGNs, whereas the 5 starburst models represent a typical range of SED types, with an extrapolation beyond $100 \mu\text{m}$ using a grey body with $\beta=1.5$. The best-fit model obtained with **DecompIR** considering the *Herschel* datapoints (Fig. 2) yields $L_{\text{IR}} = 2.2 \times 10^{12} L_{\odot}$, with AGN and starburst contributions of 53% and 47%, respectively. This allows us to recompute the SFR removing the AGN contamination. We thus obtain $\text{SFR}(\text{BCG}) = 150 \pm 15 M_{\odot} \text{ yr}^{-1}$, a value similar to that reported in Ehlert et al. (2011) but much more robust.

4.2 Mass deposition rate and SFR

MACSJ1931 harbors one of the most X-ray luminous cool cores known. The properties of the core of MACSJ1931 have been investigated in detail in Ehlert et al. (2011), where an equivalent mass deposition rate of $\sim 700 M_{\odot} \text{ yr}^{-1}$ in the inner 70 kpc has been estimated in the assumption of isobaric cooling. Despite the high cooling rate, this cluster is missing the central metallicity peak which is otherwise measured in the majority of CC clusters (DeGrandi et al. 2004). This suggests bulk transport of cool gas out to large distances from the centre due to the powerful AGN outburst (Ehlert et al. 2011). In particular, a bright, dense region north of the BCG shows low-temperature and high-density metal-rich gas and is consistent with being a remnant of the cool core after it was disrupted by the AGN (see also Kirkpatrick 2011).

We constrain the ICM mass cooling rate, \dot{M} , in the inner 30 kpc around the BCG under the same assumption of isobaric cooling. The main difference relative to the previ-

ous analysis by Ehlert et al. (2011) is that we focus on a limited temperature range, 0.15–3.0 keV, and in particular below 1.8 keV. In fact, the signature of an isobaric cooling flow is given by a specific relation between the emission measure and the gas temperature, as described in the model **mkcflow** (Mushotzky et al. 1988). Therefore we measure the cooling rate of the gas independently in five temperature bins, using a set of **mkcflow** models within XSPEC (Arnaud et al. 1996) in the following temperature intervals: 0.15–0.25, 0.25–0.45, 0.45–0.9, 0.9–1.8, 1.8–3.0 keV. We also consider a single temperature **mekal** (Mewe et al. 1985, 1986; Kaastra et al. 1992; Liedahl et al. 1995) component to account for the gas hotter than 3 keV. We detect about 13700 net counts (0.5–7.0 keV band) in the inner 30 kpc. Since it is not possible to measure the metal abundance of the cold gas, given its low emission measure, we conservatively assume that its metallicity is equal to that of the **mekal** component which dominates the emission, which is $Z = 0.35 \pm 0.05 Z_{\odot}$. We find that the mass deposition rate for gas below 3 keV has a 95% single-sided upper limit of $\dot{M} < 135 M_{\odot} \text{ yr}^{-1}$ (see dashed horizontal line in Fig. 3, left panel), while the temperature of the **mekal** component is $kT = 6.43^{+0.50}_{-0.45} \text{ keV}$. When we try to constrain \dot{M} in temperature intervals, we find that we are able to measure a substantial mass deposition rate only in the temperature range 1.8–3.0 keV. Below 1.8 keV, the upper limit on the mass deposition rate is only $\dot{M} < 58 M_{\odot} \text{ yr}^{-1}$ at a 95% c.l. The upper limits measured in different temperature bins are shown in Fig. 3, left panel. We find that \dot{M} is significantly lower - at least by a factor 3 - than the measured SFR.

This result is in broad agreement with the correlation between the SFR observed in the BCG and the properties of the hosting cool core (Rafferty et al. 2006; Rawle et al. 2012), but in disagreement with previous measurements of a mass deposition rate typically higher than the SFR in the BCG (Odea 2006; McDonald2011 et al. 2011; Mittal et al. 2015). Clearly, the ratio of the mass deposition rate and the SFR is sensitive to the times scales for ICM cooling and star formation and it is not expected to vary much among clusters. To check whether we can reconcile the results for MACSJ1931 with previous results, we also explore the presence of colder clouds (with temperature $< 10^7 \text{ K}$) in the ICM beyond 30 kpc, where a significant fraction of colder gas can cool and fall into the innermost regions. This is suggested by a recent work by Voit et al. (2015) which showed that colder clouds can precipitate out of the hot gas via thermal instability on a large region centered in the core, feeding black hole accretion and/or star formation in the BCG. Even in this case we find an upper limit (95% c.l.) of 45 and $52 M_{\odot} \text{ yr}^{-1}$ in annuli of 30–50 and 50–70 kpc, respectively. Therefore, we do not find evidence of a large amount of colder gas within 30 kpc nor falling from beyond 30 kpc onto the centre. The low upper limits on the mass deposition rate found in the case of MACSJ1931, may require a scenario where the time scale for star formation rate in the BCG is longer than the cooling events occurring intermittently in the cluster core. To investigate this possibility, we are currently exploring the relation between \dot{M} and SFR in a small sample of nearby clusters whose BCG shows significant star formation (Molendi et al. in preparation).

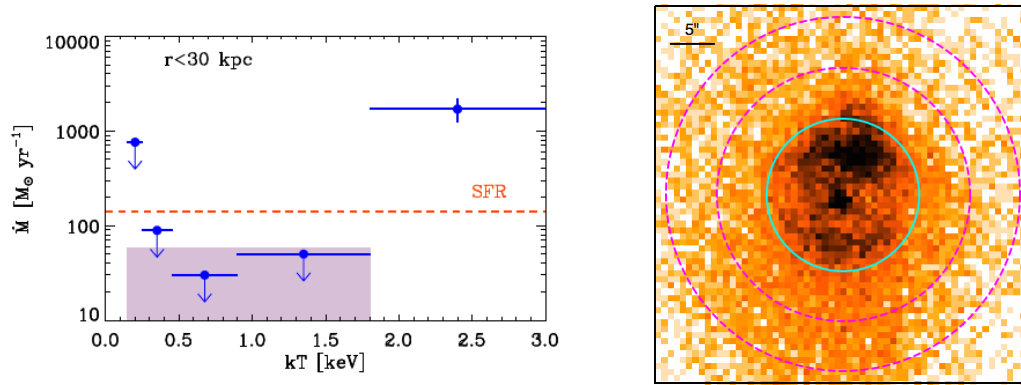


Figure 3. *Left* \dot{M}/M_{\odot} (blue circles) measured in different temperature bins in the inner 30 kpc of MACJ1931. Errors bars correspond to 1σ while arrows indicate single-sided 95% upper limits. The shaded area is the single-sided 95% upper limit on the global mass cooling rate obtained with a single `mkcflow` model in the temperature range 0.15 – 1.8 keV. The horizontal line marks the star formation rate of the BCG. *Right* Soft X-ray band ($0.5' \times 0.5'$) centered on the BCG. The regions in which we computed \dot{M} are shown in cyan (inner 30 kpc) and in magenta (annulus with 50 – 70 kpc radius). North is up and East to the left.

5 CONCLUSIONS

In this Letter, we present a study of the dust obscured star formation properties in the galaxy cluster MACS1931 at $z=0.352$, and a detailed investigation on the origin of the BCG SFR. We detect FIR emission in 6 cluster members and we derive SFRs based on broad band FIR SEDs in the range 5 - 150 $M_{\odot}\text{yr}^{-1}$, and dust temperatures in the range 24-33 K. The strongest *Herschel* source in the cluster field is, notably, the BCG, one of the few ULIRGs detected in the nearby Universe. Our analysis shows the importance of adequately assessing the contamination from AGN, but even accounting for $\sim 50\%$ of L_{IR} due to the AGN we estimate a $\text{SFR}=150 M_{\odot}\text{yr}^{-1}$ for the BCG, a surprising value for a galaxy expected to be “red & dead”. At similar redshift only Abell 1835 has a comparable SFR. At the same time, cold gas ($kT < 1.8$ keV) is not detected in the ICM gas, and the mass deposition rate has a robust upper limit of $58 M_{\odot}\text{yr}^{-1}$, suggesting that in this case star formation lasts longer than the ICM cooling events.

ACKNOWLEDGEMENTS

We thank G. Risaliti, G. Giovannini, E. Liuzzo and M. Massardi for useful discussions on the AGN properties. We also thank the anonymous referee for useful comments. JSS and IB acknowledge funding from the European Union Seventh Framework Programme (FP7/2007-2013) under grant agreement nr 267251 “Astronomy Fellowships in Italy” (AstroFit). We acknowledge financial support from PRIN INAF 2012 *A unique dataset to address the most compelling open questions about X-ray galaxy clusters* and PRIN-INAF 2014: *Glittering Kaleidoscopes in the sky, the multifaceted nature and role of galaxy clusters*. Results are partly based on ESO LP186.A-0798. *Herschel* is an ESA space observatory with science instruments provided by European-led PI consortia and with important participation from NASA.

REFERENCES

- Arnaud, K.A., 1996, ASP Conf.Ser., 101, Astronomical Data Analysis Software and Systems V, 5, 17
 Arnouts, S., et al., 1999, MNRAS, 310, 540
 Bertin, E., & Arnouts, S. 1996, A&AS, 117, 393
 Balog, Z., et al. 2014, Experimental Astronomy, 37, 129
 Chary, R., & Elbaz, D. 2001, ApJ, 556, 562
 De Grandi, S., Ettori, S., Longhetti, M., & Molendi, S. 2004, A&A, 419, 7
 Donahue, M., et al. 2014, ApJ, 794, 136
 Donahue, M., et al. 2015, ApJ, 805, 177
 Dressler, A. 1980, ApJ, 236, 351
 Dressler, A., et al. 1997, ApJ, 490, 577
 Ebeling, H., et al. 2001, ApJ, 548, L23
 Ehlert, S., et al. 2011, MNRAS, 411, 1641
 Fogarty, K., Postman, M., Connor, T., Donahue, M., & Moustakas, J. 2015, arXiv:1509.00487
 Hoffer, A. S., Donahue, M., Hicks, A., & Barthelmy, R. S. 2012, ApJS, 199, 23
 Girardi, M., et al. 2015, A&A, 579, A4
 Gnedin, O. Y. 2003, ApJ, 589, 752
 Griffin, M. J., et al. 2010, A&A, 518, L3
 Hao, C.-N., et al. 2011, ApJ, 741, 124
 Hudson, D. S., et al. 2010, A&A, 513, A37
 Hlavacek-Larrondo, J. et al. 2013, MNRAS, 431, 1638
 Kaastra, J.S. 1992, An X-Ray Spectral Code for Optically Thin Plasmas (Internal SRON-Leiden Report, updated version 2.0)
 Kennicutt R. C., Jr, 1998, ARA&A, 36, 189
 Kennicutt, R. C., & Evans, N. J. 2012, ARA&A, 50, 531
 Kirkpatrick, C. C., McNamara, B. R., & Cavagnolo, K. W. 2011, ApJ, 731, L23
 Kroupa, P., & Weidner, C. 2003, ApJ, 598, 1076
 Liedahl, D. A., Osterheld, A. L., & Goldstein, W. H. 1995, ApJ, 438, L115
 Magdis, G., et al. 2014 ApJ 796 63
 McDonald, M., et al. 2011, ApJ, 734, 95
 McDonald, M., et al. 2012, Nature, 488, 349
 McNamara, B. R., & Nulsen, P. E. J. 2007, ARA&A, 45, 117
 Merten, J., et al. 2015, ApJ, 806, 4
 Mewe, R., Gronenschild, E. H. B. M., & van den Oord, G. H. J. 1985, A&AS, 62, 197
 Mewe, R., Lemen, J. R., & van den Oord, G. H. J. 1986, A&AS, 65, 511
 Mittal, R., et al. 2015, MNRAS, 450, 2564
 Moore, B., et al. 1996, Nature, 379, 613
 Mullaney, J. R., et al. 2011, MNRAS, 414, 1082
 Murphy, E. J., et al. 2011, ApJ, 737, 67
 Mushotzky, R. F., & Szymkowiak, A. E. 1988, NATO Advanced Science Institutes (ASI) Series C, 229, 53
 O’Dea, C. P., et al., 2008, ApJ, 681, 1035
 Peterson, J. R., Fabian, A. C., 2006. Phys. Rep. 427:139
 Piazzo, L., et al. 2015, MNRAS, 447, 1471

- Pilbratt, G. L., et al. 2010, A&A, 518, L1
 Poglitsch, A., et al. 2010, A&A, 518, L2
 Popesso, P., et al. 2015, A&A, 579, A132
 Postman, M., et al. 2012, ApJS, 199, 25
 Rafferty, D. A., McNamara, B. R., Nulsen, P. E. J., & Wise, M. W. 2006, ApJ, 652, 216
 Rawle, T. D., et al. 2012, ApJ, 747, 29
 Rosati, P., et al. 2014, The Messenger, 158, 48
 Roseboom I., et al. 2012, MNRAS, 419, 2758
 Russell, H. R. et al. 2013, MNRAS, 432, 530
 Samuele, R., et al. 2011, ApJ, 731, 31
 Voit, G. M., et al. 2015, Nature, 519, 203
 von der Linden, A., et al., 2010, MNRAS, 404, 1231